ACS OMEGA

Open Access

http://pubs.acs.org/journal/acsodf

Article

Probing the Structural Degradation of $CsPbBr_3$ Perovskite Nanocrystals in the Presence of H_2O and H_2S: How Weak Interactions and HSAB Matter

Karayadi H. Fausia,[#] Bijoy Nharangatt,[#] Ramachandran Nair Vinayakan, Analiparambil R. Ramesh, Vijayan Santhi, Kuppathil R. Dhandapani, Thathamkulam Prabhakaran Manoj, Raghu Chatanathodi, Deepthi Jose,* and Kulangara Sandeep*

Cite This: *ACS Omega* 2024, 9, 8417−8424

Read Online

ACCESS | Metrics & More | Article Recommendations | Supporting Information

ABSTRACT: Structural degradation of all inorganic $CsPbBr_3$ in the presence of moisture is considered as one of its major limitations to use as an active component in various light-harvesting and light-emitting devices. Herein, we used two similar molecules, H_2O and H_2S, with similar structures, to follow the decomposition mechanism of $CsPbBr_3$ perovskite nanocrystals. Interestingly, H_2O acts as a catalyst for the decomposition of $CsPbBr_3$, which is in contrast to H_2S. Our experimental observations followed by density functional theory (DFT) calculations showed that the water molecule is intercalated in the $CsPbBr_3$ perovskite whereas H_2S is adsorbed in the (100) planes of $CsPbBr_3$ by a weak electrostatic interaction. According to Pearson's hard−soft acid−base theory, both cations present in $CsPbBr_3$ prefer soft/intermediate bases. In the case of the water molecule, it lacks a soft base and thus it is not directly involved in the reaction whereas H_2S can provide a soft base and thus it gets involved in the reaction. Understanding the mechanistic aspects of decomposition can give different methodologies for preventing such unwanted reactions.

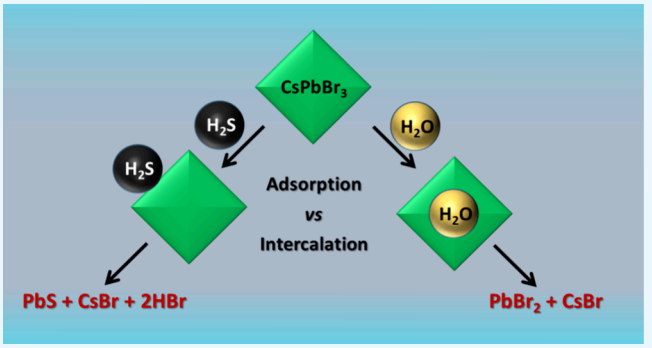

INTRODUCTION

The search for new materials for efficient and cost-effective harvesting of light energy has been hovering around lead halide perovskites for the past decade, owing to their high extinction coefficient, absorption in a broad wavelength range, and large exciton diffusion lengths.[1−6] More interestingly, the emission of lead halide perovskites can be tuned in the entire visible region, by postsynthetic anion exchange reaction, in an easier manner.[7−11] The emission quantum yield of the lead halide perovskites is close to unity and also shows an exceptional electroluminescent yield with a fairly narrow emission profile.[12−14] Thus, lead halide perovskites are proposed as an alternate material for the fabrication of light-emitting diodes (LED), display devices, and sensors.[9,15−20] Apart from this, lead halide perovskite is the one of the materials that showed a commendable efficiency for solar cells, so far, in the laboratory.[21−23] Many of the interesting properties of lead halide perovskites are attributed to their peculiar crystal structure.[24−27] Even though lead halide perovskite proved its efficiency for various applications, the stability under ambient conditions is a major concern.[28−33] Lead halide perovskites are known to decompose in the presence of small molecules like water.[34] Water is also known to be used as a greener solvent for the synthesis of lead halide perovskites at moderately high temperatures.[35,36] In order to improve the stability of lead halide perovskites under ambient conditions, especially in humid atmospheres, the exact mechanism of moisture-assisted decomposition needs to be understood. One way to analyze the mechanism is to use structurally and chemically similar molecules and treat them with a lead halide perovskite lattice under identical conditions. Herein, we have chosen two molecules, H_2O (water) and H_2S (hydrogen sulfide), and the structural transformations of cesium lead halide perovskites in the presence of these molecules are investigated. All inorganic $CsPbBr_3$ is known for its exceptional properties and various applications.[36,37] H_2O and H_2S molecules are hydrides of the chalcogen (XVI[th] group in the periodic table) group elements and have similar chemical structures. In the case of $CsPbBr_3$, it decomposes to $PbBr_2$ and CsBr in the presence of water

Received: December 1, 2023
Revised: January 6, 2024
Accepted: January 11, 2024
Published: February 7, 2024

molecules.[37] During the decomposition of three-dimensional $CsPbBr_3$ perovskites, a $CsPb_2Br_5$ sheet is formed as the intermediate.[38−42] Walsh and co-workers theoretically demonstrated that the surface adsorption (hydration) followed by the intercalation of water/solvent molecules in the interstitial sites is the reason for the structural degradation of methylammonium lead halide perovskites upon moisture exposure.[43,44] Some of the structural transformations of perovskites are reversible, and the physical insights on such equilibria can give better understanding of the formation/decomposition of lead halide perovskites. For the current investigation, all inorganic $CsPbBr_3$ perovskite is taken, as it is known for exceptional properties, and its decomposition in the presence of water and hydrogen sulfide molecules is investigated experimentally and theoretically.

RESULTS AND DISCUSSION

The $CsPbBr_3$ perovskite nanocrystals are prepared by following a previous report with slight modifications.[45] The details of the preparation and purification of all inorganic $CsPbBr_3$ perovskite nanocrystals are provided in Experimental Section. Oleylamine (OAm) and oleic acid (OA) are the capping agents used for the preparation of nanocrystals, which facilitated the dispersion of $CsPbBr_3$ nanocrystals in nonpolar organic solvents.[46,47] Furthermore, the purified $CsPbBr_3$ perovskite nanocrystals are characterized using spectroscopic methods, X-ray diffraction, and electron microscopy. The quantum confined nature of the $CsPbBr_3$ nanocrystals is confirmed by the presence of the excitonic peak in the UV−vis electronic absorption spectrum (Figure 1A). Nanocrystals used in the present investigation exhibited the first excitonic peak at 508 nm, which is the measure of minimum energy electronic transition. Furthermore, the nanocrystals are characterized by emission spectroscopy. The emission spectrum of the purified $CsPbBr_3$ nanocrystals exhibited a symmetrical Gaussian-like profile centered at 517 nm, with a full width at half-maximum (FWHM) of 19 nm (Figure 1B). The red shift in emission from the excitonic absorption is well known in the literature.[48] The emission spectrum is recorded by exciting the samples at 350 nm by keeping the slit widths in the emission and excitation chambers at 1 nm. The shorter FWHM is a clear indication that the synthesized nanocrystals are monodispersed with fewer surface defects.[49−52] Furthermore, the emission yield of the perovskite nanocrystals is obtained by following a relative method. The aqueous solution of fluorescein dye in 0.1 N NaOH (quantum yield 0.925) is used as the standard, and the quantum yield of the present perovskite nanocrystals is estimated as 0.55. The details of the quantum yield measurements are provided in Experimental Section. All the electronic UV−visible spectroscopic measurements are carried by dissolving $CsPbBr_3$ nanocrystals in chloroform by using quartz cuvettes having a path length of 1 cm. Furthermore, transmission electron microscopy (TEM) is used to image the perovskite nanocrystals. The low-resolution TEM analysis confirms the crystallinity and monodispersity of the perovskite nanocrystals (Figure S1A, SI). The average size of the nanocrystals can be obtained by a size distribution histogram. It is determined as 8.1 nm for the present $CsPbBr_3$ perovskite nanocrystals. The details are given in Figure S1B of the Supporting Information (SI). The schematic representation of the crystal structure of $CsPbBr_3$ perovskite is presented in Figure 1C. Furthermore, high-resolution TEM analysis is carried out and the results are presented in Figure 1D and SI. The d-spacing value along the z-axis is estimated with high-resolution TEM using Gatan DigitalMicrograph software. The d-spacing value obtained from the high-resolution TEM is 0.58 nm, which corresponds to the (100) planes of the cubic perovskite structure. Furthermore, the crystalline nature of the samples is characterized using powder X-ray diffraction (PXRD) (Figure 1E). The perovskite samples are found to be particularly monocrystalline, providing a significant diffraction domain that establishes good crystalline nature. The powder XRD pattern of the sample is found at 2θ values 15.4 and 31.08°, which are the perfect matches to the (100) and (200) crystalline planes of the cubic perovskite crystals (Figure 2A). The obtained values are in good agreement with the XRD spectrum of the cubic $CsPbBr_3$ perovskites as per joint committee for powder diffraction standards.[40]

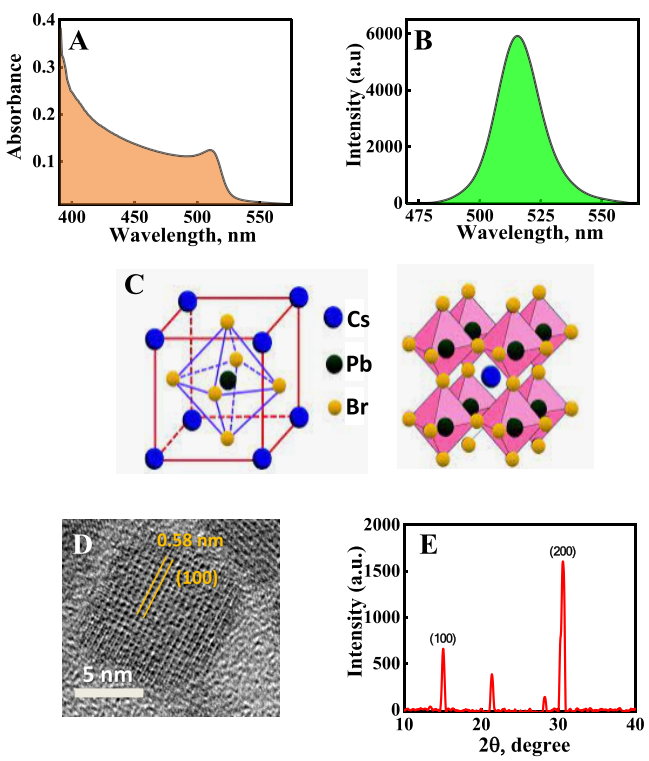

Figure 1. Characterization of $CsPbBr_3$ perovskites: (A) absorption, (B) emission spectrum taken in chloroform, (C) schematic representation of the crystal structure of $CsPbBr_3$ perovskite nanocrystals, (D) high-resolution TEM image that contains the d-spacing analysis, and (E) X-ray diffraction pattern.

In order to understand the mechanism of decomposition, we studied the reactions of $CsPbBr_3$ perovskite nanocrystals in the presence of H_2O and H_2S The experiment was carried out by bubbling the H_2O and H_2S gas, individually, through the $CsPbBr_3$ perovskite taken in chloroform for 5 min. Both the gases are slightly soluble in chloroform. The solubility of water in chloroform is 8%, and that of H_2S is 5%.[40] In both cases, $CsPbBr_3$ perovskite nanocrystals underwent decomposition. In the presence of water vapor, the decomposed product is a white precipitate whereas the decomposed product in the presence of H_2S is a brownish black precipitate.[40,53] Photographs of the decomposed products are presented in the SI (Figure S2). Under identical conditions, H_2O is passed from a pressure cooker and H_2S is passed from the Kipps apparatus. Both the residues obtained after the decomposition are

https://doi.org/10.1021/acsomega.3c09600
ACS Omega 2024, 9, 8417−8424

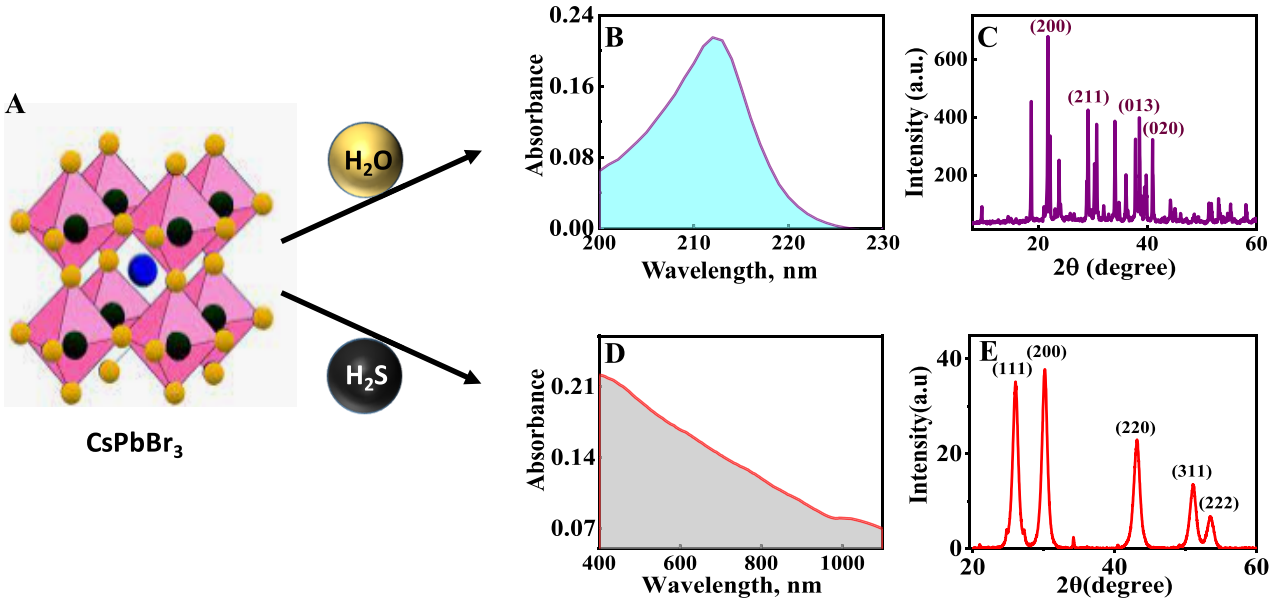

Figure 2. (A) Schematic representation showing the reaction of $CsPbBr_3$ with water and hydrogen sulfide. (B) Absorption spectrum and (C) powder XRD pattern of the $PbBr_2$ formed after the decomposition of $CsPbBr_3$ in the presence of H_2O. (D) The absorption and (E) PXRD patterns of the PbS formed after the decomposition of $CsPbBr_3$.

separated by centrifugation and washed with water. Furthermore, the precipitates and the water washings are characterized using qualitative techniques. Absorption spectra of the products after the reaction with H_2O and H_2S are presented as Figure 2B and D, respectively. The PXRD pattern confirmed that the white residue formed after the decomposition of $CsPbBr_3$ perovskite nanocrystals in the presence of H_2O is $PbBr_2$ (Figure 2C) and the precipitate formed in the presence of H_2S is lead sulfide (Figure 2D). The diffraction patterns of $PbBr_2$ (card file no. 31-0679) and PbS (card file no. 05-0592) match those of the Joint Committee on Powder Diffraction Standards. The XRD pattern of the decomposed product after washing with chloroform in the presence of water is presented in Figure S3. It clearly indicates the formation of CsBr. In both cases, the aqueous washings showed the presence of cesium and bromide ions by qualitative analysis. Details of the analysis are given in the SI. Apart from this, the pH of water washings of the decomposed product in the presence of H_2S is found to be slightly acidic, in contrast to the decomposition in the presence of moisture. From the experimental observations, the $CsPbBr_3$ perovskite nanocrystals decompose in the presence of H_2O and H_2S as per eqs 1 and 2, respectively.

$$CsPbBr_3 + H_2O \rightarrow PbBr_2 + CsBr + H_2O \quad (1)$$

$$CsPbBr_3 + H_2S \rightarrow PbS + 2HBr + CsBr \quad (2)$$

Even though H_2O and H_2S molecules have similar structures, they react with $CsPbBr_3$ in a totally different manner. In the case of H_2O, it acts as a catalyst for the decomposition of $CsPbBr_3$ perovskite nanocrystals. At the same time, H_2S is involved in the reaction. However, in the case of methylammonium lead halide perovskites, water is involved in the reaction.[54] Furthermore, the formation enthalpies of the possible reactions are calculated. The formation enthalpy of PbO is 438 kJ/mol, that of PbS is −100.4 kJ/mol, and that of $PbBr_2$ is −278.7 kJ/mol. It is clear that the formation of PbO is not preferred, from the formation enthalpy, in the presence of water, and the most stable product is $PbBr_2$. However, in the presence of H_2S, the formed product is PbS, even though the formation of both the $PbBr_2$ and PbS is possible. Among $PbBr_2$ and PbS, the kinetically favored product is PbS.

To understand the differential behavior of $CsPbBr_3$ toward H_2O and H_2S, we employed DFT calculations using the Vienna Ab initio Simulation Package (VASP).[55−58] The electron−ion interaction was represented through the projector augmented wave (PAW) method.[56] The generalized gradient approximation (GGA)-based PBE functional was used to approximate the exchange correlation.[57] Grimme's dispersion corrections were incorporated into these calculations to achieve a precise prediction of adsorption geometry of molecules, in alignment with experimental results.[59] The solutions of Kohn−Sham equations are expanded in a plane-wave basis set with a kinetic energy cutoff of 500 eV. A 3 × 3 supercell of the $CsPbBr_3$ (100) surface was used to calculate surface adsorption, and a cubic structure ($a = b = c$ and $\alpha = \beta = \gamma = 90°$) of $CsPbBr_3$ was taken in order to study the intercalation interaction. A regular 10 × 10 × 10 and 4 × 4 × 1 mesh centered at the gamma point are used for sampling the Brillouin zone for bulk and surface calculations, respectively. A vacuum of more than 20 Å is ensured along the c-axis to rule out any interaction between the periodic images for surface calculations.

We calculated the intercalation energy by

$$E_{int} = E_{CsPbBr_3 \cdot H_2X} - (E_{CsPbBr_3} + E_{H_2X}) \quad (3)$$

where $E_{CsPbBr_3 \cdot H_2X}$, E_{CsPbBr_3}, and E_{H_2X} are the total energies of the intercalated bulk, the cubic bulk unit cell per formula unit, and an isolated H_2X (X = S, O) molecule, respectively.

The adsorption energy is calculated using the formula

$$E_{ads} = E_{final} - (E_{surf} + E_{H_2X}) \quad (4)$$

https://doi.org/10.1021/acsomega.3c09600
ACS Omega 2024, 9, 8417−8424

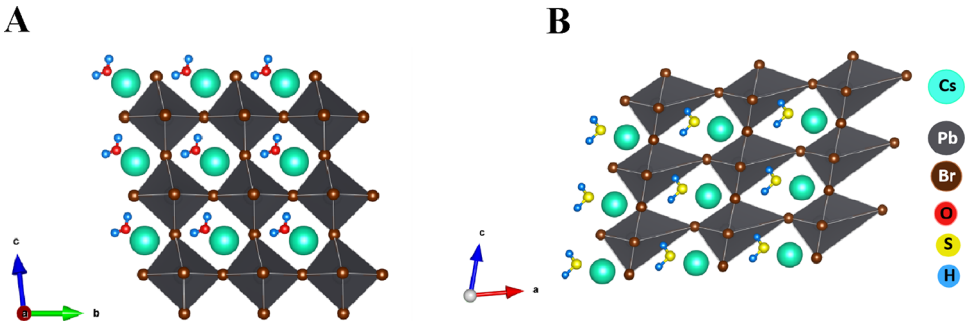

Figure 3. Optimized geometry $CsPbBr_3$ intercalated with (A) H_2O and (B) H_2S molecules.

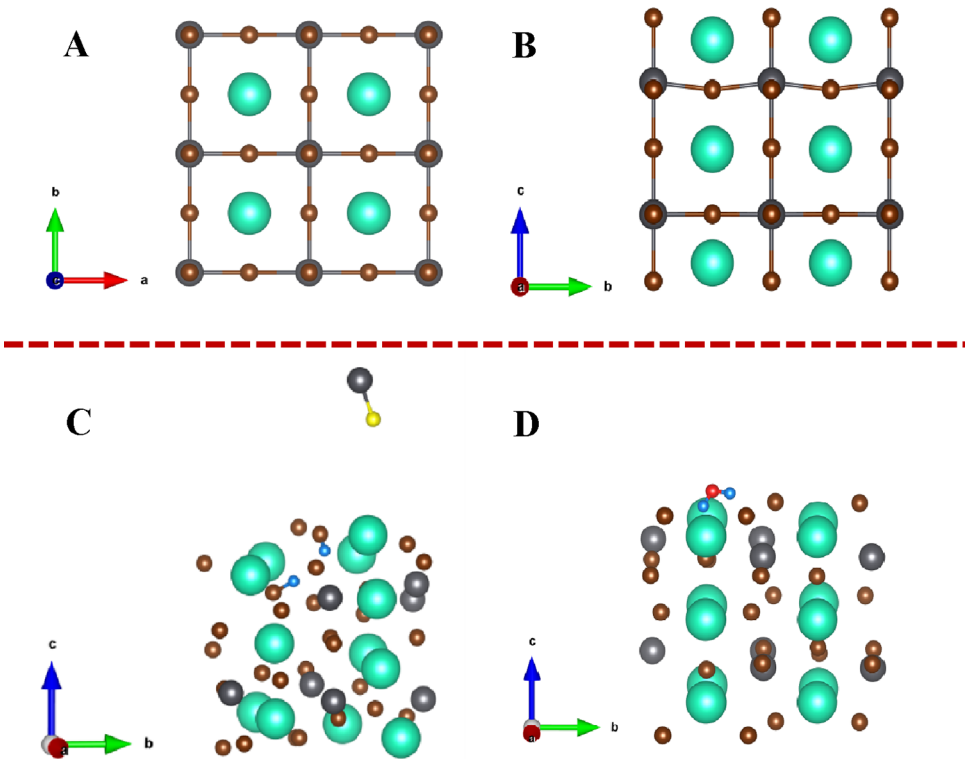

Figure 4. Relaxed geometry of the $CsPbBr_3$ (001) surface, (A) top and (B) side views. The optimized geometry of (C) H_2S and (D) H_2O adsorbed on the $CsPbBr_3$ (001) surface.

where E_{final}, E_{surf}, and E_{H_2X} are the energy of the adsorbed state, $CsPbBr_3$ (001) surface, and H_2X (X = S, O) molecules, respectively.

The optimized lattice parameter of the cubic structure is found to be 5.98 Å. Initially, we considered the intercalation of both H_2S and H_2O into the $CsPbBr_3$ unit cell and found that both molecules successfully intercalate into the $CsPbBr_3$ bulk. The intercalation energies for H_2O and H_2S were calculated to be −0.70 and −0.12 eV, respectively. The geometry of the bulk system after intercalation with H_2O and H_2S is shown in Figure 3. The negative intercalation energy for H_2O indicates the intercalation of water molecules into $CsPbBr_3$ bulk consistent with previous reports.[43] The intercalation of H_2S induced significant disruption in the CsPbBr3 bulk with 23.68% expansion in volume. Conversely, H_2O intercalation led to a shrinkage of the volume by 6.57%.

To investigate the nature of the interatomic interaction between the perovskite and the molecules, we calculated the Bader charge on each atom. The Bader charges of Cs and Pb atoms were calculated to be −0.88e and −1.07e, respectively, while each Br shows a Bader charge of 0.64e. The H atoms of the water molecule have Bader charges of −0.61e and −0.57e, respectively, and the O atom has a Bader charge of 1.19e. Consequently, the strong attraction between O atom and Cs atom results in the compression of the volume of $CsPbBr_3$ during intercalation of the water molecule. A significant alteration occurred in the Cs−Br interaction distance, decreasing to 3.61 Å after intercalation, compared to that of the pristine $CsPbBr_3$ where it was 4.23 Å, falling within the range expected for Cs−Br ionic bonds. This redistribution of charges during intercalation might have caused the dissociation of $CsPbBr_3$ to the observed products. However, in the case of H_2S, two H atoms have a very negligible Bader charge and S has a Bader charge of 0.02e. The interatomic attraction between H_2S and $CsPbBr_3$ is relatively weak compared to those of H_2O and $CsPbBr_3$. Hence, the unit cell expands to accommodate the H_2S molecule resulting in the expansion of the volume upon H_2S intercalation into $CsPbBr_3$. To further validate the assumption that both the size and the polarity of the intercalating molecule are decisive factors in the

https://doi.org/10.1021/acsomega.3c09600
ACS Omega 2024, 9, 8417−8424

intercalation process, we conducted intercalation calculations using D_2O and SO_2. A volume shrinkage of 6.36% was observed during D_2O intercalation, which is comparable to that of water. Notably, despite SO_2 being a larger molecule than H_2S in size, the greater dipole moment of SO_2 leads to the shrinkage in volume of $CsPbBr_3$ by 2.25%.

To examine the potential formation of $PbBr_2$ and PbS through H_2O intercalation and H_2S intercalation, respectively, we calculated the formation energy for $PbBr_2$ ($E_{F(PbBr2)}$) and PbS ($E_{F(PbS)}$) using the following formulas:

$$E_{F(PbBr2)} = (E_{CsBr} + E_{PbBr_2} + E_{H_2O}) - E_{CsPbBr_3 \cdot H_2O} \quad (5)$$

$$E_{F(PbS)} = (E_{CsBr} + E_{PbS} + 2^*E_{HBr}) - E_{CsPbBr_3 \cdot H_2S} \quad (6)$$

The formation energy of $PbBr_2$ was calculated to be −0.14 eV indicating the formation of $PbBr_2$ through H_2O intercalation by following the known literature report.[55] On the other hand, the positive value of 0.48 eV for the formation energy of PbS suggests that the intercalation of H_2S does not result in the experimentally observed formation of PbS. Therefore, we opted to explore the behavior of H_2S and H_2O at the surface of $CsPbBr_3$. We did the adsorption on different phases of the $CsPbBr_3$ (001) surface, and the one that supports the experimental observation is reported here. The optimized geometry of the $CsPbBr_3$ (001) surface that contains both Cs and Br atoms is shown in Figure 4. In the bulk $CsPbBr_3$, all Pb−Br bond lengths have the same bond length, 2.99 Å. However, in the $CsPbBr_3$ (001) phase under consideration, three distinct Pb−Br bonds were observed.

The in-plane Pb−Br bond length measured 3.04 Å with two distinct types of out-of-plane Pb−Br bond lengths that are shorter than the P−Br bond length in the bulk. The out-of-plane Pb−Br bond length exposed on the surface was found to be 2.84 Å, but the out-of-plane Pb−Br bond length inside the network measured 2.91 Å. Every Br atom in the $CsPbBr_3$ bulk is bonded to two Pb atoms that results in a stable Pb−Br network, but on the $CsPbBr_3$ (001) surface, only one Pb atom is connected to the surface Br atoms. Hence, the Bader charge on the surface Br atoms increased to 0.65e while the Bader charge of Br atoms inside the network decreased to 0.60e. The reduction in the coordination number of Cs atoms on the surface also resulted in an anisotropic charge distribution in the system.

The relaxed geometry of H_2S and H_2O adsorbed on the $CsPbBr_3$ (001) phase is shown in Figure 4C,D. The adsorption of H_2O on the $CsPbBr_3$ (001) surface distorted it significantly, but the H_2O molecule remained intact with an O−H bond length of 0.98 Å. Thus, the H_2O molecule can intercalate into the bulk with an increase in its concentration. The adsorption energy for H_2O on the $CsPbBr_3$ (001) surface was calculated to be −2.16 eV. Upon adsorption, the H_2S molecules undergo dissociation on the $CsPbBr_3$ (001) surface leading to the formation of PbS and two HBr molecules, as shown in Figure 4C, in agreement with the experimentally observed results. The Pb−S bond length is found to be 2.33 Å, and the H−Br bond lengths are found to be 1.45 and 1.59 Å. The formation energy of the PbS unit was calculated using eq 7.

$$E_{F(PbS)} = (E_{PbS} + E_{residue}) - E_{CsPbBr_3+H_2S} \quad (7)$$

Since PbS is formed as an isolated unit after adsorption, we have considered it as the major product and the rest we refer as the residue. Here, $E_{F(PbS)}$ is the formation energy of PbS, E_{PbS} is the energy of a single PbS unit, $E_{residue}$ is the energy of the residue, and $E_{CsPbBr_3+H_2S}$ is the energy of H_2S adsorbed on the $CsPbBr_3$ (100) surface. The formation energy was calculated to be −2.45 eV, which suggests the formation of PbS by H_2S adsorption on the surface. The anisotropic charge distribution on the (001) surface could be the reason for the dissociation of H_2S on the (001) surface. These interactions can be explained by employing Pearson's hard−soft acid−base (HSAB) theory. According to this theory, the cations in the hard category prefer to interact with the anions from the same category and the soft cations form stable products with soft anions.[60] Based on the charge and size of the ions, they are classified into hard and soft. In $CsPbBr_3$, Cs^+ is classified in the soft acid category and the Pb^{2+} in borderline acid inclines more toward softer. In an earlier work, we have demonstrated the inclination of Pb^{2+} ions in $CsPbBr^3$, more toward the soft base side by taking chloride and iodide ions.[60] In the presence of equal numbers of Cl^- and I^-, the Pb^{2+} in the lead halide perovskites preferentially interact with the iodide ions.[60] In the case of H_2O, both the ion proton and the hydroxyl ions are known as hard due to their high charge density and less polarizable nature. For the decomposition reaction of $CsPbBr_3$ with water, the anions present in the reaction medium are hydroxide and bromide ions. Both the cations, Cs^+ and Pb^{2+}, prefer bromide ions to form stable salts as a result of the HSAB principle.

CONCLUSIONS

In conclusion, our experimental observations along with DFT calculations suggest that the structural degradation of $CsPbBr_3$ perovskite nanocrystals follows different mechanisms, in contrast to methylammonium lead halide perovskites, in the presence of H_2O and H_2S molecules. The adsorption of H_2S on the surface of $CsPbBr_3$ perovskite degrades the crystal structure and leads to the products PbS, HBr, and CsBr. The mere adsorption of water on $CsPbBr_3$ (100) does not show any evidence for the formation of experimentally observed products. The decomposition of $CsPbBr_3$ perovskite by water possibly involves adsorption, followed by intercalation. The HSAB principle plays a crucial role on dictating the mechanism of decomposition. Both of the cations present in the $CsPbBr_3$ prefer to form salt with moderate/soft bases. In the case of water-induced decomposition, the intercalation takes place, which causes the structural degradation, whereas in the presence of H_2S, the decomposition of $CsPbBr_3$ takes place at the surface by the adsorption. The mechanistic aspects discussed in the structural degradation of $CsPbBr_3$ in the presence of H_2O and H_2S can give new insights into stabilizing lead halide perovskites in the presence of small molecules. Better understanding of the decomposition mechanism can lead to the formulation of new methodologies to stabilize $CsPbBr_3$ perovskites.

EXPERIMENTAL SECTION

Synthesis of $CsPbBr_3$ Perovskite Nanocrystals. The synthesis of all inorganic cesium lead bromide perovskite nanocrystals is carried out by following reported procedures with slight modifications.[45] The procedure involves two steps. In the initial step, cesium-oleate is prepared by the reaction of chemicals cesium carbonate and OA in a three-neck round-bottom flask under an inert atmosphere. The reagents cesium carbonate and OA are allowed to react in a 1:2 molar ratio at 120 °C to get an optically clear solution corresponding to Cs-

https://doi.org/10.1021/acsomega.3c09600
ACS Omega 2024, 9, 8417−8424

oleate. High vacuum is applied in between to remove gaseous byproducts carbon dioxide and water. In another R.B. flask, lead bromide ($PbBr_2$, 0.19 mmol, 69.73 mg) is heated with capping ligands oleyl amine (1.14 mmol, 1.6 mL) and oleic acid (0.5 mmol, 0.15 mL) in the solvent octadecene (3 mL), under a nitrogen atmosphere of 150 °C to get the lead-oleyl amine complex. The Cs-oleate (0.046 mmol), synthesized in the initial step, is quickly injected to this complex at 170 °C to get $CsPbBr_3$ perovskite nanocrystals. The perovskite nanocrystals are purified by repeated precipitation and washing with spectroscopic grade acetone followed by the centrifugation.

Emission Quantum Yield Measurement. The photoluminescence quantum yield of the present $CsPbBr_3$ perovskite nanocrystals is estimated by a relative method. Fluorescein dye dissolved in 0.1 M NaOH (Φ_{ST}: 0.9) is used as the standard. The Equation 8 is used for the calculation of emission quantum yield.

$$\Phi_x = \Phi_{ST}(f_x/f_{ST})(a_{ST}/a_X)(n_x^2/n_{ST}^2) \quad (8)$$

where f_x = emission area of the sample, f_{ST} = emission area of the standard reference, n_x = refractive index of the solvent used for the emission measurement of $CsPbBr_3$, n_{ST} = refractive index of the solvent used for the emission measurement of the standard dye fluorescein, a_{ST} = absorbance of the reference standard at the excitation wavelength, a_X = absorbance of the sample at the excitation wavelength, and Φ_{ST} = quantum yield of the standard dye.

■ ASSOCIATED CONTENT

Supporting Information

The Supporting Information is available free of charge at https://pubs.acs.org/doi/10.1021/acsomega.3c09600.

Materials, methods, synthesis of $CsPbBr_3$ nanocrystals, characterization, low-resolution TEM analysis, emission yield measurements, photographs of the precipitates formed after the decomposition of $CsPbBr_3$ in the presence of H_2S and H_2O, qualitative tests, PXRD of the decomposed product in the presence of water, optimized geometry of the (001) plane, and intercalation studies in the $CsPbBr_3$ bulk structure (PDF)

■ AUTHOR INFORMATION

Corresponding Authors

Deepthi Jose − *Department of Chemistry, Providence Women's College, Calicut 673009, India*; Email: deepthijose@providencecollegecalicut.ac.in

Kulangara Sandeep − *Government Victoria College, Research Center under University of Calicut, Palakkad 678001, India*; orcid.org/0000-0002-4275-3495; Email: sandeepk@gvc.ac.in

Authors

Karayadi H. Fausia − *Government Victoria College, Research Center under University of Calicut, Palakkad 678001, India*

Bijoy Nharangatt − *Department of Physics, National Institute of Technology, Calicut, Kerala 673601, India*

Ramachandran Nair Vinayakan − *Department of Kerala Chemistry, N.S.S. Hindu College, Changanassery 686102, India*; orcid.org/0000-0003-0082-3659

Analiparambil R. Ramesh − *Government Victoria College, Research Center under University of Calicut, Palakkad 678001, India*

Vijayan Santhi − *Government Victoria College, Research Center under University of Calicut, Palakkad 678001, India*

Kuppathil R. Dhandapani − *Government Victoria College, Research Center under University of Calicut, Palakkad 678001, India*

Thathamkulam Prabhakaran Manoj − *Government Victoria College, Research Center under University of Calicut, Palakkad 678001, India*

Raghu Chatanathodi − *Department of Physics, National Institute of Technology, Calicut, Kerala 673601, India*; orcid.org/0000-0001-9649-8285

Complete contact information is available at: https://pubs.acs.org/10.1021/acsomega.3c09600

Author Contributions

#K.H.F. and B.N. contributed equally to this paper.

Notes

The authors declare no competing financial interest.

■ ACKNOWLEDGMENTS

The authors thank Professor K. George Thomas from Indian Institutes of Science Education and Research Thiruvananthapuram (IISER-TVM), for the continuous support and encouragement. K.H.F., A.R.R., V.S., K.R.D., T.P.M., and K.S. thank DST-FIST (award number: SR/FST/325/2016) for the funding. D.J. acknowledges the support of SERB-TARE (award number: TAR/2018/000637) and the DBT STAR College scheme for the funding. The authors acknowledge the Center for Computational Modeling and Simulation (CCMS), NIT Calicut, for the computational support. The authors acknowledge St. Thomas College Thrissur for XRD measurements.

■ REFERENCES

(1) Manser, J. S.; Christians, J. A.; Kamat, P. V. Intriguing Optoelectronic Properties of Metal Halide Perovskites. *Chem. Rev.* **2016**, *116*, 12956−13008.

(2) De Roo, J.; Ibáñez, M.; Geiregat, P.; Nedelcu, G.; Walravens, W.; Maes, J.; Martins, J. C.; Van Driessche, I.; Kovalenko, M. V.; Hens, Z. Highly Dynamic Ligand Binding and Light Absorption Coefficient of Cesium Lead Bromide Perovskite Nanocrystals. *ACS Nano* **2016**, *10*, 2071−2081.

(3) Deng, S.; Shi, E.; Yuan, L.; Jin, L.; Dou, L.; Huang, L. Long-range Exciton Transport and Slow Annihilation in Two-dimensional Hybrid Perovskites. *Nat. Commun.* **2020**, *11* (1), 664.

(4) Dey, A.; Ye, J.; De, A.; Debroye, E.; Ha, S. K.; Bladt, E.; Kshirsagar, A. S.; Wang, Z.; Yin, J.; et al. State of the Art and Prospects for Halide Perovskite Nanocrystals. *ACS Nano* **2021**, *15*, 10775−10981.

(5) Chouhan, L.; Ghimire, S.; Subrahmanyam, C.; Miyasaka, T.; Biju, V. Synthesis, Optoelectronic Properties and Applications of Halide Perovskites. *Chem. Soc. Rev.* **2020**, *49*, 2869−2885.

(6) De Trizio, L.; Infante, I.; Manna, L. Surface Chemistry of Lead Halide Perovskite Colloidal Nanocrystals. *Acc. Chem. Res.* **2023**, *56*, 1815−1825.

(7) Sakhatskyi, K.; John, R. A.; Guerrero, A.; Tsarev, S.; Sabisch, S.; Das, T.; Matt, G. J.; Yakunin, S.; Cherniukh, I.; Kotyrba, M.; et al. Assessing the Drawbacks and Benefits of Ion Migration in Lead Halide Perovskites. *ACS Energy Lett.* **2022**, *7*, 3401−3414.

(8) Protesescu, L.; Yakunin, S.; Bodnarchuk, M. I.; Krieg, F.; Caputo, R.; Hendon, C. H.; Yang, R. X.; Walsh, A.; Kovalenko, M. V. Nanocrystals of Cesium Lead Halide Perovskites ($CsPbX_3$, X = Cl, Br, and I): Novel Optoelectronic Materials Showing Bright Emission with Wide Color Gamut. *Nano Lett.* **2015**, *15*, 3692−3696.

(9) Sandeep, K.; Padmakumar, K.; Ambili, K. U.; Jishnu, P.; Fousia, K. H.; Ramesh, A. R.; Rappai, J. P.; Santhi, V.; Shanthil, M. Anion Exchange in Lead Halide Perovskites: An Overview. *Phys. Status Solidi B* **2022**, *259*, No. 2100600.
(10) Li, J.; Han, Z.; Liu, J.; Zou, Y.; Xu, X. Compositional Gradient Engineering and Applications in Halide Perovskites. *Chem. Commun.* **2023**, *59*, 5156−5173.
(11) Evarestov, R. A.; Kotomin, E. A.; Senocrate, A.; Kremer, R. K.; Maier, J. First-principles Comparative Study of Perfect and Defective $CsPbX_3$ (X = Br, I) crystals. *Phys. Chem. Chem. Phys.* **2020**, *22*, 3914−3920.
(12) Li, X.; Gao, X.; Zhang, X.; Shen, X.; Lu, M.; Wu, J.; Shi, Z.; Colvin, V. L.; Hu, J.; Bai, X.; Yu, W. W.; Zhang, Y. Lead-Free Halide Perovskites for Light Emission: Recent Advances and Perspectives. *Adv. Sci.* **2021**, *8*, No. 2003334.
(13) Swarnkar, A.; Chulliyil, R.; Ravi, V. K.; Irfanullah, M.; Chowdhury, A.; Nag, A. Colloidal $CsPbBr_3$ Perovskite Nanocrystals: Luminescence beyond Traditional Quantum Dots. *Angew. Chem., Int. Ed.* **2015**, *54*, 15424−15428.
(14) Ezzeldien, M.; Al-Qaisi, S.; Alrowaili, Z. A.; Alzaid, M.; Maskar, E.; Es-Smairi, A.; Vu, T. V.; Rai, D. P. Electronic and Optical Properties of Bulk and Surface of $CsPbBr_3$ Inorganic Halide Perovskite a First Principles DFT 1/2 Approach. *Sci. Rep.* **2021**, *11*, 20622.
(15) George, K. J.; Halali, V. V.; Sanjayan, C. G.; Suvina, V.; Sakar, M.; Balakrishna, R. G. Perovskite Nanomaterials as Optical and Electrochemical Sensors. *Inorg. Chem. Front.* **2020**, *7*, 2702−2725.
(16) Sandeep, K.; Hamida, K. T. $CsPbBr_3$ Perovskite−Coated Paper Substrate for the Cost-Effective Detection of Fluoride, Chloride, and Iodide Ions in Water. *Phys. Status Solidi A* **2021**, *218*, No. 2100101.
(17) Sandeep, K. $CsPbBr_3$ Perovskite Nanocrystals Coated Paper Substrate as Atmospheric Humidity Sensor. *Mater. Today: Proc.* **2021**, *41*, 610−612.
(18) Woo, S.-J.; Kim, J. S.; Lee, T.-W. Characterization of Stability and Challenges to Improve Lifetime in Perovskite LEDs. *Nat. Photonics* **2021**, *15*, 630−634.
(19) Tawil, C. A.; Kurdi, R. E.; Patra, D. Cesium Lead Bromide Perovskites: Synthesis, Stability, and Photoluminescence Quantum Yield Enhancement by Hexadecyltrimethylammonium Bromide Doping. *ACS Omega* **2022**, *7*, 20872−20880.
(20) Tang, J.; Tian, W.; Zhao, C.; Sun, Q.; Zhang, C.; Cheng, H.; Shi, Y.; Jin, S. Imaging the Moisture-Induced Degradation Process of 2D Organolead Halide Perovskites. *ACS Omega* **2022**, *7*, 10365−10371.
(21) Guo, Z.; Jena, A. K.; Kim, G. M.; Miyasaka, T. The High Open-Circuit Voltage of Perovskite Solar Cells: a Review. *Energy Environ. Sci.* **2022**, *15*, 3171−3222.
(22) Gollino, L.; Leblanc, A.; Dittmer, J.; Mercier, N.; Pauporté, T. New Dication-Based Lead-Deficient 3D MAPbI3 and $FAPbI_3$ "d-HPs" Perovskites with Enhanced Stability. *ACS Omega* **2023**, *8*, 23870−23879.
(23) Chen, R.; Du, J.; Zheng, X.; Yang, Y.; Yuan, L.; Yang, Y.; Li, F.; Wang, H. Molecule Stapling-Assisted Fabrication of High-quality $CsPbI_2Br$ films for Efficient and Stable Photovoltaic Modules. *J. Mater. Chem. A* **2023**, *11*, 13371−13377.
(24) Sandeep, K. Revealing the Role of Aggregation and Surface Chemistry in the Bi-phasic Anion Exchange Reactions of Cesium Lead Halide Perovskites. *ChemistrySelect* **2020**, *5*, 4034−4039.
(25) Garai, A.; Vishnu, E. K.; Banerjee, S.; Nair, A. A. K.; Bera, S.; Thomas, K. G.; Pradhan, N. Vertex-Oriented Cube-Connected Pattern in $CsPbBr_3$ Perovskite Nanorods and Their Optical Properties: An Ensemble to Single-Particle Study. *J. Am. Chem. Soc.* **2023**, *145*, 13989−13999.
(26) Zhao, H.; Wang, Y.; Wang, C.; Bandela, A. K.; Thumu, U. Dissolution-Dictated Recrystallization in Cesium Lead Halide Perovskites and Size Engineering in δ-$CsPbI_3$ Nanostructures. *Cryst. Growth Des.* **2023**, *23*, 7412−7423.
(27) Pascazio, R.; Zaccaria, F.; van Beek, B.; Infante, I. Classical Force-Field Parameters for $CsPbBr_3$ Perovskite Nanocrystals. *J. Phys. Chem. C* **2022**, *126*, 9898−9908.
(28) Chowdhury, T. A.; Bin Zafar, M. A.; Sajjad-Ul Islam, M.; Shahinuzzaman, M.; Islam, M. A.; Khandaker, M. U. Stability of Perovskite Solar Cells: Issues and Prospects. *RSC Adv.* **2023**, *13*, 1787−1810.
(29) Schmitz, F.; Lago, N.; Fagiolari, L.; Burkhart, J.; Cester, A.; Polo, A.; Prato, M.; Meneghesso, G.; Gross, S.; Bella, F.; Lamberti, F.; Gatti, T. High Open-Circuit Voltage $Cs_2AgBiBr_6$ Carbon-Based Perovskite Solar Cells via Green Processing of Ultrasonic Spray-Coated Carbon Electrodes from Waste Tire Sources. *ChemSusChem* **2022**, *15*, No. e202201590.
(30) Tian, F.; Feng, W.; Xing, B.; He, X.; Saidi, W. A.; Zhang, L. Grain Boundaries in Methylammonium Lead Halide Perovskites Facilitate Water Diffusion. *Adv. Energy Sustainability Res.* **2021**, *2*, No. 2100087.
(31) Idígoras, J.; Aparicio, F. J.; Contreras-Bernal, B.; Ramos-Terrón, S.; Alcaire, M.; Sánchez-Valencia, J. R.; Borras, A.; Barranco, A.; Anta, J. A. Enhancing Moisture and Water Resistance in Perovskite Solar Cells by Encapsulation with Ultrathin Plasma Polymers. *ACS Appl. Mater. Interfaces* **2018**, *10*, 11587−11594.
(32) Xiong, J.; Qi, Y.; Zhang, Q.; Box, D.; Williams, K.; Tatum, J.; Das, P.; Pradhan, N. R.; Dai, Q. Enhanced Moisture and Water Resistance in Inverted Perovskite Solar Cells by Poly(3-hexylthiophene) *ACS Appl. Energy Mater.* **2021**, *4*, 1815−1823.
(33) Ruan, P.; Zhang, W.; Cheng, F.; Zhang, W.; Yin, J.; Li, J.; Zheng, N.; Chen, R.; Hui, Y.; Wu, B.; Wang, Y.; Huang, X.; Xu, Z. Moisture-Tolerant and High-Quality α-$CsPbI_3$ Films for Efficient and Stable Perovskite Solar Modules. *J. Mater. Chem. A* **2020**, *8*, 9597−9606.
(34) Zhou, X.; Xin, C.; Hou, F.; Shi, B.; Pan, S.; Hou, S.; Zhang, J.; Wang, P.; Ren, H.; Zhao, Y.; Wang, G.; Li, Y.; Zhang, H. Role of Moisture in the Preparation of Efficient Planar Perovskite Solar Cells. *ACS Sustainable Chem. Eng.* **2019**, *7* (21), 17691−17696.
(35) Tang, X.; Kothalawala, N. L.; Zhang, Y.; Qian, D.; Kim, D. Y.; Yang, F. Water-Driven $CsPbBr_3$ Nanocrystals and Poly(Methyl Methacrylate)-$CsPbBr_3$ Nanocrystal Films with Bending-Endurable Photoluminescence. *J. Chem. Eng.* **2021**, *425*, No. 131456.
(36) Tang, X.; Zhang, Y.; Kothalawala, N. L.; Wen, X.; Kim, D. Y.; Yang, F. $MAPbBr_3$ Nanocrystals from Aqueous Solution for Poly(Methyl Methacrylate)-$MAPbBr_3$ Nanocrystal Films with Compression-Resistant Photoluminescence. *Nanotechnology* **2022**, *33*, No. 235605.
(37) Chakkamalayath, J.; Hiott, N.; Kamat, P. V. How Stable Is the 2D/3D Interface of Metal Halide Perovskite under Light and Heat? *ACS Energy Lett.* **2023**, *8*, 169−171.
(38) Sanjayan, C. G.; Jyothi, M. S.; Balakrishna, R. G. Stabilization of $CsPbBr_3$ Quantum Dots for Photocatalysis, Imaging and Optical Sensing in Water and Biological Medium: a Review. *J. Mater. Chem. C* **2022**, *10*, 6935−6956.
(39) Pradhan, N. Journey of Making Cesium Lead Halide Perovskite Nanocrystals: What's Next. *J. Phys. Chem. Lett.* **2019**, *10*, 5847−5855.
(40) Sandeep, K.; Gopika, K. Y.; Revathi, M. R. Role of Capped Oleyl Amine in the Moisture-Induced Structural Transformation of $CsPbBr_3$ Perovskite Nanocrystals. *Phys. Status Solidi RRL* **2019**, *13*, No. 1900387.
(41) Bera, S.; Behera, R. K.; Das Adhikari, S.; Guria, A. K.; Pradhan, N. Equilibriums in Formation of Lead Halide Perovskite Nanocrystals. *J. Phys. Chem. Lett.* **2021**, *12*, 11824−11833.
(42) Li, M.; Peng, S.; Fang, S.; Gong, Y.; Yang, D.; Bu, K.; Liu, B.; Luo, H.; Guo, S.; Li, J.; Wang, H.; Liu, Y.; Jiang, S.; Lin, C.; Lü, X. Synthesis of Two-Dimensional $CsPb_2X_5$ (X = Br and I) with a Stable Structure and Tunable Bandgap by $CsPbX_3$ Phase Separation. *J. Phys. Chem. Lett.* **2022**, *13*, 2555−2562.
(43) Jong, U.-G.; Yu, C.-J.; Ri, G.-C.; McMahon, A. P.; Harrison, N. M.; Barnes, P. R. F.; Walsh, A. Influence of Water Intercalation and Hydration on Chemical Decomposition and Ion Transport in

https://doi.org/10.1021/acsomega.3c09600
ACS Omega 2024, 9, 8417−8424

Methylammonium Lead Halide Perovskites. *J. Mater. Chem. A* **2018**, *6*, 1067−1074.
(44) Shin, M.; Kim, J.; Jung, Y.-K.; Ruoko, T.-p.; Priimagi, A.; Walsh, A.; Shin, B. Low-Dimensional Formamidinium Lead Perovskite Architectures via Controllable Solvent Intercalation. *J. Mater. Chem. C* **2019**, *7*, 3945−3951.
(45) Sandeep, K.; Reshmi, C. P. Modulating the Emission of $CsPbBr_3$ perovskite nanocrystals via thermally varying magnetic field of $La_{0.67}Sr_{0.33}Mn_{0.9}(Ni/Co)_{0.1}O_3$. *AIP Adv.* **2020**, *10*, No. 035302.
(46) Abiodun, S. L.; Gee, M. Y.; Greytak, A. B. Combined NMR and Isothermal Titration Calorimetry Investigation Resolves Conditions for Ligand Exchange and Phase Transformation in $CsPbBr_3$ Nanocrystals. *J. Phys. Chem. C* **2021**, *125*, 17897−17905.
(47) Sandeep, K.; Sabrin, H. I.; Divya, P.; Gopika, K. Y.; Fausia, K. H.; Shanthil, M. Overcoming the Photoinduced Solvent-Assisted Anion Exchange Reactions of $CsPbBr_3$ Perovskite Nanocrystals. *J. Phys. Chem. C* **2023**, *127*, 14495−14501.
(48) Baranov, D.; Toso, S.; Imran, M.; Manna, L. Investigation into the Photoluminescence Red Shift in Cesium Lead Bromide Nanocrystal Superlattices. *J. Phys. Chem. Lett.* **2019**, *10*, 655−660.
(49) Vishnu, E. K.; Kumar Nair, A. A.; Thomas, K. G. Core-Size-Dependent Trapping and Detrapping Dynamics in CdSe/CdS/ZnS Quantum Dots. *J. Phys. Chem. C* **2021**, *125*, 25706−25716.
(50) Mandal, S.; Ghosh, S.; Mukherjee, S.; Roy, D.; De, C. K.; Mukhuti, K.; Mandal, P. K. Near-Ergodic $CsPbBr_3$ Perovskite Nanocrystal with Minimal Statistical Aging. *J. Phys. Chem. Lett.* **2021**, *12*, 10169−10174.
(51) Paul, S.; Kishore, G.; Samanta, A. Photoluminescence Blinking of Quantum Confined $CsPbBr_3$ Perovskite Nanocrystals: Influence of Size. *J. Phys. Chem. C* **2023**, *127*, 10207−10214.
(52) Ahmed, T.; Paul, S.; Samanta, A. Photoluminescence Blinking Revealing Static and Dynamic Heterogeneity of the Hole Transfer Process in Phenothiazine-Adsorbed $FAPbBr_3$ Single Nanocrystals. *J. Phys. Chem. C* **2022**, *126*, 9109−9116.
(53) Chen, C.; Cai, Q.; Luo, F.; Dong, N.; Guo, L.; Qiu, B.; Lin, Z. Sensitive Fluorescent Sensor for Hydrogen Sulfide in Rat Brain Microdialysis via $CsPbBr_3$ Quantum Dots. *Anal. Chem.* **2019**, *91*, 15915−15921.
(54) Tolouei nia, P.; Khassaf, H.; Shirazi Amin, A.; Tobin, Z. M.; Alpay, S. P.; Suib, S. L. Moisture-Induced Structural Degradation in Methylammonium Lead Iodide Perovskite Thin Films. *ACS Appl. Energy Mater.* **2020**, *3*, 8240−8248.
(55) Kresse, G.; Hafner, J. Ab initio Molecular Dynamics for Liquid Metals. *Phys. Rev. B* **1993**, *47*, 558−561.
(56) Kresse, G.; Furthmüller, J. Efficient Iterative Schemes for ab initio Total-energy Calculations using a Plane-Wave Basis Set. *Phys. Rev. B* **1996**, *54*, 11169−11186.
(57) Kresse, G.; Joubert, D. From Ultrasoft Pseudopotentials to the Projector Augmented-wave Method. *Phys. Rev. B* **1999**, *59*, 1758−1775.
(58) Perdew, J. P.; Burke, K.; Ernzerhof, M. Generalized Gradient Approximation Made Simple [Phys. Rev. Lett. 77, 3865 (1996)]. *Phys. Rev. Lett.* **1997**, *78*, 1396−1396.
(59) Grimme, S. Semiempirical GGA-type Density Functional Constructed with a Long-Range Dispersion Correction. *J. Comput. Chem.* **2006**, *27*, 1787−1799.
(60) Divya, P.; Anagha, G.; Nharangatt, B.; Chatanathodi, R.; Sabrin, H.; Nourin, N.; Fausia, K. H.; Padmakumar, K.; Jose, D.; Sandeep, K. Anion Exchange Reaction of $CsPbBr_3$ Perovskite Nanocrystals: Affinity of Halide Ion Matters. *ChemistrySelect* **2022**, *7*, No. e202203868.

https://doi.org/10.1021/acsomega.3c09600
ACS Omega 2024, 9, 8417−8424